

# BLO-Inst: Bi-Level Optimization Based Alignment of YOLO and SAM for Robust Instance Segmentation

Li Zhang<sup>1</sup> Pengtao Xie<sup>1</sup>

## Abstract

The Segment Anything Model has revolutionized image segmentation with its zero-shot capabilities, yet its reliance on manual prompts hinders fully automated deployment. While integrating object detectors as prompt generators offers a pathway to automation, existing pipelines suffer from two fundamental limitations: objective mismatch, where detectors optimized for geometric localization do not correspond to the optimal prompting context required by SAM, and alignment overfitting in standard joint training, where the detector simply memorizes specific prompt adjustments for training samples rather than learning a generalizable policy. To bridge this gap, we introduce BLO-Inst, a unified framework that aligns detection and segmentation objectives by bi-level optimization. We formulate the alignment as a nested optimization problem over disjoint data splits. In the lower level, the SAM is fine-tuned to maximize segmentation fidelity given the current detection proposals on a subset ( $D_1$ ). In the upper level, the detector is updated to generate bounding boxes that explicitly minimize the validation loss of the fine-tuned SAM on a separate subset ( $D_2$ ). This effectively transforms the detector into a segmentation-aware prompt generator, optimizing the bounding boxes not just for localization accuracy, but for downstream mask quality. Extensive experiments demonstrate that BLO-Inst achieves superior performance, outperforming standard baselines on tasks in general and biomedical domains. The anonymous code of BLO-Inst is available at <https://github.com/importZL/BLO-Inst>.

## 1. Introduction

Instance segmentation, the task of detecting and outlining individual objects in an image, is a core requirement for applications ranging from autonomous driving to biomedical analysis (Yi et al., 2019; Zhou et al., 2020). Traditionally, this field relied on specialized models trained for specific tasks, such as Mask R-CNN (He et al., 2017) and SOLO (Wang et al., 2021). However, these approaches often suffer from limited generalization and require training with large annotated datasets. In contrast, the emergence of foundation models has fundamentally shifted this landscape (Benigmim et al., 2024; Zhou et al., 2025) for their enriched prior knowledge. The Segment Anything Model (SAM) (Kirillov et al., 2023) serves as a robust foundation model trained on 11 million images to handle diverse tasks without retraining. Unlike traditional methods, SAM operates as a promptable method, generating high-quality masks from prompts like points or boxes. While this design is ideal for interactive segmentation, it presents a bottleneck for automated pipelines where human input is infeasible (Li et al., 2025). Consequently, deploying SAM for autonomous instance segmentation requires replacing manual guidance with a detector capable of self-generating accurate prompts.

To achieve automation, a common strategy is to combine SAM with object detectors (e.g., YOLO (Redmon et al., 2016) and DINO (Liu et al., 2024)) in a sequential pipeline, where the detector provides bounding boxes as prompts. However, simply using a pretrained detector suffers from a fundamental objective mismatch, as the box that fits the target object perfectly is often not the best prompt for creating a good mask. For instance, as shown in Figure 2, a pedestrian might need a tighter box to remove background noise, while a cell might need a larger box to capture intact structure. To address this, recent works like USIS-SAM (Lian et al., 2024) and RSPrompter (Chen et al., 2024) attempt to train the detector and SAM together based on the sum of segmentation and detection losses. While this enables the detector to output desired prompts for mask decoder, it leads to another limitation: alignment overfitting. In this standard setup, the detector and segmenter are trained on the exact same data examples. This causes the detector to simply memorize the specific box adjustments needed to

<sup>1</sup>Electrical and Computer Engineering, University of California San Diego, CA, US. Correspondence to: Pengtao Xie <p1xie@ucsd.edu>.

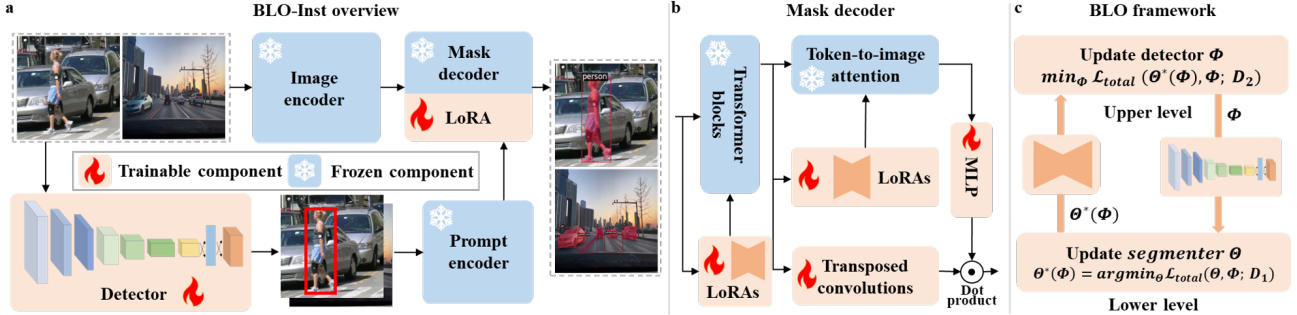


Figure 1. Overview of the BLO-Inst framework. (a) The architecture combines a trainable YOLO detector (parameters  $\Phi$ ) with the Segment Anything Model (SAM). (b) We employ Parameter-Efficient Fine-Tuning (PEFT) by freezing SAM’s heavy encoder and injecting learnable LoRA layers (parameters  $\Theta$ ) into the mask decoder. (c) The Bi-Level Optimization process: the lower level updates the segmenter  $\Theta$  on  $D_1$  to maximize mask fidelity given fixed prompts, while the upper level updates the detector  $\Phi$  on  $D_2$  to generate prompts that minimize the segmenter’s validation loss.

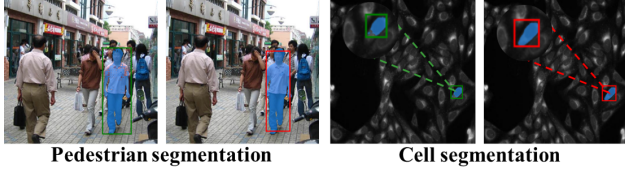


Figure 2. Illustration of the objective mismatch. Pedestrian (Left): A tighter box (Red) outperforms the precise one (Green) by reducing background clutter. Cell (Right): A larger box (Red) outperforms the precise one (Green) by providing essential context.

minimize the loss for those training samples, rather than learning a general rule for creating good prompts for the mask decoder. Consequently, when applied to new images during testing, this memorized alignment may break down, resulting in sub-optimal segmentation. Such limitation can also be experimentally observed through the performance gap between “standard single-level optimization” and “bi-level optimization” in the ablation study that explore the impact on optimization strategy.

To address these limitations, we draw inspiration from the standard machine learning strategy of hyper-parameter tuning (Kim & Hospedales, 2025). In machine learning, hyper-parameters are typically tuned on a separate validation set to ensure they maximize the model’s generalization capability, rather than overfitting to the training set. We apply this same strategy to the design of our framework. We regard the bounding boxes provided by the detector not merely as static prompts for mask decoder, but as “dynamic hyper-parameters” generated by the detector that guide the prediction of the mask decoder. If the detector is optimized on the same data as the segmenter, it would overfit the prompts to that specific training set, similar to how tuning hyper-parameters on training data leads to poor generalization. However, by treating the detector as a set of hyper-parameters and optimizing it based on the segmenter’s response on a separate validation split, we enforce a overfitting-resistant alignment. This shifts the learning objective from simply finding the object to finding the optimal prompt for the segmenter, thereby resolving the objective mismatch and alignment overfitting simultaneously.

Realizing this concept, we introduce BLO-Inst, a unified framework that implements this strategy via bi-level optimization (BLO) (Choe et al., 2022). Specifically, as shown in Figure 1(a), BLO-Inst manages two sets of parameters: the segmentation model (including LoRA layers (Hu et al., 2021) and original MLP heads, while keeping the heavy image encoder to be frozen) and the object detector. We formulate the training process as a nested optimization problem over two disjoint subsets of the training data ( $D_1$  and  $D_2$ ), as illustrated in Figure 1(c). In the lower level, we tentatively fix the object detector and fine-tune the SAM on the subset ( $D_1$ ) to maximize segmentation performance given the current detector. In the upper level, we validate the fine-tuned SAM on another subset ( $D_2$ ) and update the detector. The objective of the upper level is to generate prompts that minimize the validation loss. This ensures the detector is optimized to generate prompts that help SAM segment new images correctly. By segregating the learning processes onto distinct data subsets, BLO-Inst effectively mitigates the risk of alignment overfitting, ensuring the detector learns a robust, generalizable prompting policy.

Our contributions are summarized as follows:

- We identify the alignment overfitting in current automated segmentation pipelines where standard joint training causes detectors to memorize training data rather than learning generalizable prompting strategies for a specific task.
- We propose BLO-Inst, a bi-level optimization framework that formulates the detector’s weights as meta-parameters. By optimizing the detector on a separate validation split, we effectively prevent alignment overfitting, ensuring the model learns robust prompting rules that generalize to unseen data rather than memorizing training distributions.
- Extensive experiments across general and biomedical domains validate that BLO-Inst achieves superior performance, outperforming standard joint-training baselines and architectural modification approaches.

## 2. Related Work

### 2.1. Instance Segmentation

Instance segmentation is a core computer vision challenge that unifies object detection and semantic segmentation, requiring the model to not only localize objects of interest but also delineate their precise pixel-level boundaries (Liu et al., 2018b; Yang et al., 2023). Traditionally, deep learning approaches have been dominated by two-stage frameworks, epitomized by Mask R-CNN (He et al., 2017). These methods operate by first generating candidate region proposals by a Region Proposal Network (RPN) (Ren et al., 2015) and subsequently performing fine-grained classification and mask generation using mechanisms like RoIAlign (Gong et al., 2021). While highly accurate, the sequential nature of two-stage models often incurs high computational latency. To address this, one-stage architectures such as SOLO (Wang et al., 2020) and SOLOv2 (Wang et al., 2021) were developed to predict masks directly from full-image feature maps without explicit proposal generation, offering a superior trade-off between inference speed and accuracy. More recently, the field has witnessed a paradigm shift towards transformer-based architectures (Vaswani et al., 2017) like Mask2Former (Cheng et al., 2022), which formulate segmentation as a set prediction problem using learnable queries, paving the way for the prompt-based paradigms.

With the advent of vision foundation models, recent research has shifted toward utilizing the Segment Anything Model (SAM) (Kirillov et al., 2023) for instance-level tasks. While open-vocabulary detectors like GroundingDINO (Liu et al., 2024) and YOLO-World (Cheng et al., 2024) can be cascaded with SAM in a sequential pipeline, this leads to a disjoint optimization problem where the detector is optimized for box regression, while the segmenter requires prompt optimal to predict segmentation maps. To address this, recent approaches have proposed automated prompting modules. USIS-SAM (Lian et al., 2024) introduces a lightweight prompt generator trained from scratch for underwater image processing, while RSPrompter (Chen et al., 2024) attaches query-based heads to the SAM encoder for remote sensing. However, these methods typically rely on standard joint training strategies on the same dataset. As discussed, this approach suffers from alignment overfitting, the prompt generator learns to memorize specific box adjustments for the training samples rather than learning a robust, generalizable prompting policy. In contrast, our work treats the detector as a hyper-parameter and optimizes it by bi-level optimization to ensure robust alignment.

### 2.2. Foundation Model Adaptation

The emergence of large-scale foundation models has necessitated efficient strategies to adapt their generalized representations to downstream tasks without the cost of training

from scratch (Radford et al., 2018; Devlin et al., 2018). Current adaptation paradigms primarily fall into two categories: Prompt Tuning and Parameter-Efficient Fine-Tuning (PEFT). Prompt tuning methods, such as CoOp (Zhou et al., 2022) and VPT (Jia et al., 2022), introduce learnable tokens to the input space to guide the frozen model’s behavior for specific downstream tasks. Conversely, PEFT strategies like Adapters (Houlsby et al., 2019) and Low-Rank Adaptation (LoRA) (Hu et al., 2021) inject lightweight trainable modules into the model’s architecture, updating only a fraction of the parameters. In the context of the Segment Anything Model (SAM) (Kirillov et al., 2023), these strategies have been extensively explored for domain-specific applications. Approaches such as MedSAM (Wu et al., 2025), SAMed (Zhang & Liu, 2023), and BLO-SAM (Zhang et al., 2024) effectively leverage LoRA or adapter layers to adapt SAM to medical imaging modalities, significantly improving segmentation accuracy on CT and MRI data. However, these existing adaptation methods predominantly focus on class-level prediction or semantic segmentation, optimizing static weights for fixed categories. They often overlook the dynamic nature of instance segmentation, where the model must adapt to varying geometric prompts for individual objects. Our work bridges this gap by introducing a bi-level framework that simultaneously adapts the foundation model by PEFT and optimizes the prompt generator to provide task-aligned prompt guidance.

### 2.3. Bi-Level Optimization

Bi-level optimization (BLO) formulates learning as a nested problem where a lower-level optimization task is constrained by an upper-level objective (Liu et al., 2021). This framework has been widely applied to neural architecture search (Liu et al., 2018a; Hosseini et al., 2023), hyper-parameter optimization (Liu et al., 2022; Kim & Hospedales, 2025), and data reweighting (Chen et al., 2021; Zhang et al., 2025). In these applications, model parameters are typically optimized in the lower level on a training split, while meta-parameters (e.g. hyper-parameters, architectures, or sample weights) are learned in the upper level on a separate validation split to maximize generalization. Significant progress has been made in developing efficient gradient-based solvers for BLO problems. Liu et al. (2018a) introduced a finite difference approximation to estimate upper-level gradients without explicit hessian computation, while Finn et al. (2017) propose to compute the gradient updates of meta variables directly with iterative differentiation (Grazzi et al., 2020). Recently, Choe et al. (2022) developed a software framework that enables efficient gradient computation across these various approximation schemes. In this work, we leverage these efficient solvers to implement our proposed framework, adapting the BLO paradigm to align object detection with segmentation foundation models.

### 3. Method

#### 3.1. Overview of BLO-Inst

Our proposed framework, BLO-Inst, unifies the object detector (YOLO (Cheng et al., 2024)) and the segmentation model (SAM (Kirillov et al., 2023)) into a unified instance segmentation system, as shown in Figure 1. Let  $\Phi$  denote the trainable parameters of the YOLO detector (acting as the prompt generator), and  $\Theta$  denote the trainable parameters of the SAM (including PEFT modules like LoRA, and original lightweight modules). Standard approaches typically optimize these models by a summation of losses on the same dataset. However, this often leads to alignment overfitting, where the detector memorizes specific box adjustments for the training examples rather than learning a generalizable prompting policy. To resolve this, we formulate the training as a BLO problem. We partition the training data  $\mathcal{D}$  into two disjoint subsets:  $D_1$  and  $D_2$ . The learning process consists of two nested levels: for the lower level, we fix the detector  $\Phi$  and fine-tune the segmenter  $\Theta$  to adapt to the provided prompts on  $D_1$ ; for the upper level, we update the detector  $\Phi$  to generate prompts that minimize the validation loss of the fine-tuned segmenter on  $D_2$ . By validating the prompt quality on unseen data ( $D_2$ ), we force the detector to learn robust adjustment rules. The two levels of problems share the same form of loss function. The two levels are optimized iteratively until convergence, as shown in Algorithm 1.

**Preliminary.** As mentioned above, BLO-Inst builds upon two foundational architectures: YOLO (Cheng et al., 2024) and SAM (Kirillov et al., 2023). YOLO is a high-efficiency one-stage object detector that regresses bounding box coordinates and class probabilities directly from input images. We use YOLO as the prompt generator, parameterized by  $\Phi$ . SAM is a promptable segmentation foundation model comprising a heavy image encoder (ViT), a lightweight prompt encoder, and a mask decoder. It is designed to predict zero-shot masks based on the given prompts (points or boxes). In our framework, we employ SAM as the mask generator, parameterized by  $\Theta$  (specifically fine-tuning the decoder by LoRA), to produce high-fidelity masks conditioned on the boxes provided by YOLO.

#### 3.2. Bi-Level Optimization Framework

**Lower-Level Problem (Segmentation Adaptation).** In the lower level, the detector  $\Phi$  is fixed. It generates bounding boxes, which serve as prompts for the segmentation model. We optimize the segmenter parameters  $\Theta$  on  $D_1$  to minimize the unified objective  $\mathcal{L}_{total}$ , which is a weighted sum of four components, consistent with standard YOLO training but augmented with SAM’s feedback:

$$\mathcal{L}_{total} = \lambda_1 \mathcal{L}_{box} + \lambda_2 \mathcal{L}_{obj} + \lambda_3 \mathcal{L}_{cls} + \lambda_4 \mathcal{L}_{seg} \quad (1)$$

#### Algorithm 1 Optimization process for BLO-Inst

```

1: Input: Detector (YOLO)  $\Phi^{(0)}$ , Segmenter (SAM)  $\Theta^{(0)}$ , Training Data  $\mathcal{D}$ .
2: Params: Learning Rates  $\alpha, \beta$ .
3: Split  $\mathcal{D}$  into nonoverlapping  $D_1$  and  $D_2$ .
4: for  $t = 0$  to  $T - 1$  do
5:   Sample batches  $\mathcal{B}_1 \sim D_1$  and  $\mathcal{B}_2 \sim D_2$ .
6:   // Lower Level: Update Segmenter
7:   // Calculate Total Loss, but gradients only flow to  $\Theta$ 
8:    $L_{low} = \mathcal{L}_{total}(\text{YOLO}(\Phi^{(t)}), \text{SAM}(\Theta^{(t)}); \mathcal{B}_1)$ .
9:   Update  $\Theta^{(t+1)} \leftarrow \Theta^{(t)} - \alpha \nabla_{\Theta} L_{low}$ .
10:  // Upper Level: Update Detector
11:  // Calculate Total Loss, but gradients only flow to  $\Phi$ 
12:   $L_{upper} = \mathcal{L}_{total}(\text{YOLO}(\Phi^{(t)}), \text{SAM}(\Theta^{(t+1)}); \mathcal{B}_2)$ .
13:  Update  $\Phi^{(t+1)} \leftarrow \Phi^{(t)} - \beta \nabla_{\Phi} L_{upper}$ .
14: end for

```

where  $\lambda$  terms are hyper-parameters balancing the weight of each component, detailed illustration for objective function can be found in Appendix A. The lower level aims to solve the following optimization problem:

$$\Theta^*(\Phi) = \arg \min_{\Theta} \mathcal{L}_{total}(\Theta, \Phi; D_1) \quad (2)$$

Here,  $\Theta^*(\Phi)$  implies that the optimal segmentation parameters  $\Theta^*$  are dependent on the detector  $\Phi$ , as the value of the loss function relies on the quality and characteristics of the prompts generated by  $\Phi$ .

**Upper-Level Problem (Prompt Alignment).** In the upper level, we evaluate the performance of the fine-tuned segmenter  $\Theta^*(\Phi)$  on  $D_2$ . Our goal is to update the detector parameters  $\Phi$  to minimize the same unified objective  $\mathcal{L}_{total}$  on validation set,  $D_2$ , which simulates test-time evaluation. The upper level optimization problem is formulated as:

$$\Phi^* = \arg \min_{\Phi} \mathcal{L}_{total}(\Theta^*(\Phi), \Phi; D_2) \quad (3)$$

This objective forces the detector to find a solution that satisfies two conditions simultaneously: it must maintain high detection precision (via the detection loss terms) and, more importantly, it must generate generalizable prompts that minimize the validation loss of the segmenter on unseen data ( $D_2$ ) to prevent the alignment-overfitting. Unlike the lower level where  $\Phi$  is fixed, here  $\Phi$  is the active variable.

**Bi-Level Optimization Framework.** Integrating the aforementioned two optimization problems, we unify them into a cohesive bi-level optimization framework:

$$\begin{aligned} \min_{\Phi} \quad & \mathcal{L}_{total}(\Theta^*(\Phi), \Phi; D_2) \\ \text{s.t.} \quad & \Theta^*(\Phi) = \arg \min_{\Theta} \mathcal{L}_{total}(\Theta, \Phi; D_1) \end{aligned} \quad (4)$$

In this framework, the two optimization problems are deeply interdependent. The output of the lower level,  $\Theta^*(\Phi)$ ,

serves as a critical input for the upper level, representing the segmenter’s optimal adaptation to the current prompts. Conversely, the optimization variable  $\Phi$  (the detector) in the upper level acts as a condition in the lower-level objective, defining the prompt landscape on which the segmenter is trained. This nested structure decouples the prompt generation logic from specific training instances, effectively preventing alignment overfitting and ensuring the learned prompting policy is robust to new images.

### 3.3. Optimization Algorithm

We employ a gradient-based optimization algorithm to solve the bi-level problem defined in Eq. (4). Since obtaining the exact optimal solution  $\Theta^*(\Phi)$  in the lower level is computationally infeasible for every upper-level update, we adopt an efficient approximation strategy inspired by Liu et al. (2018a). As shown in Algorithm 1, instead of fully training the segmenter to convergence at each step, we approximate  $\Theta^*(\Phi)$  using a one-step gradient descent update. At iteration  $t$ , given the current detector  $\Phi^{(t)}$ , we update the segmenter parameters  $\Theta^{(t)}$  on the batch  $\mathcal{B}_1$ . Then, we use this updated surrogate  $\Theta'$  to approximate the optimal segmenter  $\Theta^*(\Phi^{(t)})$  for the subsequent upper-level update. Detailed derivations are provided in Appendix B.

## 4. Experiments

In this section, we evaluate BLO-Inst across a diverse set of instance segmentation tasks, ranging from general object detection to fine-grained part segmentation and biomedical object detection. We aim to demonstrate that our bi-level optimization framework effectively prevent overfitting when aligning the prompt generator (YOLO) with the segmenter (SAM) to outperform other specialist methods and automated prompting baselines.

### 4.1. Datasets

We evaluate BLO-Inst on 6 publicly available datasets, categorizing them into general and biomedical object benchmarks to assess domain generalization. For general object detection, we utilize PennFudanPed (Wang et al., 2007) for pedestrian segmentation, TransIns (SEG, 2023) for vehicle and laneline detection under varied conditions, WheatIns (Shehadeh, 2024) for dense agricultural object detection, and CarPartIns (Pasupa et al., 2022) for fine-grained multi-class segmentation of vehicle components. To assess performance in the biomedical domain, we employ Cell-CountIns (learning, 2024), a binary dataset for cell counting in low-contrast microscopy images, and RWCellIns (atri, 2023), a multi-class benchmark distinguishing red and white blood cells. These datasets vary significantly in scale, density, and complexity, ranging from binary to multi-class tasks, ensuring a robust evaluation across different domains.

More details about the datasets can be found in Appendix C. In our method, the training set is further randomly split into two subsets  $D_1$  and  $D_2$  with equal size. Baseline methods utilize the entire training set without any subdivision.

### 4.2. Experimental Settings

**Baselines and Metrics.** To comprehensively evaluate the effectiveness of our proposed framework, we compare BLO-Inst against a diverse set of state-of-the-art baselines categorized into two groups: (1) Specialist Instance Segmenters, including the representative two-stage Mask R-CNN (He et al., 2017) (abbreviated as “Mask R”) and the one-stage box-free SOLO (Wang et al., 2021); (2) Automated Prompting Approaches, including SAM-seg (Kirillov et al., 2023) with both Mask R-CNN (abbreviated as “SAM+B”) and Mask2Former (abbreviated as “SAM+M”) variants, which utilize pretrained specialist detectors to provide box prompts to the SAM (all parameters would be further fine-tuned on the target datasets), RSPrompter (Chen et al., 2024) with both anchor-based (abbreviated as “RS+Anchor”) and query-based (abbreviated as “RS+Query”) variants, and USIS (Lian et al., 2024), which employ auxiliary networks for prompt generation. Notably, if not specified, the mentioned abbreviations are applied to the following results presentations for both figures and tables. Following standard evaluation protocols, we report the Mean Average Precision (mAP) averaged over IoU thresholds from 0.5 to 0.95. To provide a more granular assessment of detection recall and segmentation mask fidelity, we also report  $AP_{50}$  and  $AP_{75}$ .

**Implementary Details.** We implement our framework using PyTorch, all the experiments are conducted on one NVIDIA A100 GPU. For the model architecture, we employ YOLOv7 (Redmon et al., 2016) as the prompt generator ( $\Phi$ ) and SAM ViT-B (Kirillov et al., 2023) initialized with SA-1B weights as the segmenter ( $\Theta$ ). To ensure parameter efficiency, the SAM backbone is frozen, and we fine-tune only the lightweight mask decoder via injected LoRA layers with a rank of  $r = 4$ . To ensure the detector is adapted to the specific domain before bi-level optimization, the YOLO component is pretrained on the training set of the target dataset for 100 iterations. During the bi-level optimization phase, the model is fine-tuned end-to-end for 20 epochs. We use Stochastic Gradient Descent (SGD) (Bottou, 2010) for both optimization levels, with learning rates set to  $\alpha = 1 \times 10^{-3}$  for the lower level (segmenter update) and  $\beta = 1 \times 10^{-3}$  for the upper level (detector update), adjusted via a LambdaLR scheduler. Regarding the unified objective function, the trade-off parameters are set as follows: box regression loss  $\lambda_1 = 0.3$ , objectness loss  $\lambda_2 = 0.7$ , classification loss  $\lambda_3 = 0.3$ , and segmentation loss  $\lambda_4 = 0.7$ . We assign higher weights to  $\lambda_{obj}$  and  $\lambda_{seg}$  to prioritize object discovery and final mask fidelity, while the relatively lower weights for  $\lambda_{box}$  and  $\lambda_{cls}$  leverage SAM’s inherent

Table 1. Comparison of BLO-Inst with baselines on single-class general object benchmarks. Metrics reported are Mean AP ( $mAP$ ),  $AP_{50}$ , and  $AP_{75}$  (%). Best results are highlighted in **bold**. The last three columns show the total number of model parameters, the number of trainable parameters (in millions), and the training time (in GPU hours) that calculated on PennFudanPed dataset with NVIDIA A100.

Method	PennFudanPed			WheatIns			Total Param(M)	Trainable Param(M)	Train Cost (GPU hours)
	$mAP$	$AP_{50}$	$AP_{75}$	$mAP$	$AP_{50}$	$AP_{75}$			
Mask R	46.4	81.8	49.0	48.8	81.9	64.8	41.71	41.48	0.38
SOLO	42.3	75.7	39.7	58.8	91.5	71.3	46.23	46.01	0.43
SAM+B	54.3	80.5	63.7	59.2	87.9	79.6	111.08	111.08	1.25
SAM+M	54.1	78.9	61.3	60.4	88.1	75.9	112.18	112.18	2.48
RS+Anchor	41.1	68.4	45.9	62.9	87.0	78.3	117.05	117.05	0.43
RS+Query	53.3	76.3	62.4	63.7	86.1	79.7	100.99	100.99	1.43
USIS	55.1	72.6	61.0	62.5	88.5	80.3	698.10	57.02	0.68
<b>BLO-Inst</b>	<b>59.3</b>	<b>86.9</b>	<b>67.8</b>	<b>68.4</b>	<b>95.6</b>	<b>84.0</b>	131.63	38.66	0.51

Table 2. Comparison of BLO-Inst with baselines on multi-class general object benchmarks. Metrics reported are Mean AP ( $mAP$ ),  $AP_{50}$ , and  $AP_{75}$  (%). Best results are highlighted in **bold**.

Method	TransIns			CarPartsIns		
	$mAP$	$AP_{50}$	$AP_{75}$	$mAP$	$AP_{50}$	$AP_{75}$
Mask R	37.7	65.5	38.4	34.0	61.7	34.9
SOLO	47.4	78.8	49.1	49.1	77.7	51.7
SAM+B	57.8	86.6	53.1	58.4	79.6	64.2
SAM+M	54.9	81.5	57.0	61.7	80.8	64.0
RS+Anchor	57.3	88.3	59.9	54.5	73.9	58.8
RS+Query	55.7	82.5	59.2	61.1	80.6	64.7
USIS	38.8	65.5	38.9	57.9	83.5	61.1
<b>BLO-Inst</b>	<b>58.8</b>	<b>90.2</b>	<b>62.2</b>	<b>65.2</b>	<b>86.5</b>	<b>67.2</b>

robustness to approximate spatial prompts, reducing the need for pixel-perfect bounding box regression. To facilitate the bi-level optimization, we randomly partition the training set into two disjoint subsets of equal size, denoted as the subsets  $D_1$  (for optimizing  $\Theta$ ) and  $D_2$  (for optimizing  $\Phi$ ).

### 4.3. Results and Analysis

**Single-class General Object Benchmarks.** We first evaluate BLO-Inst on single-class segmentation tasks using the PennFudanPed and WheatIns datasets. The quantitative results, along with model complexity and training costs, are presented in Table 1. We can see that BLO-Inst achieves the highest  $mAP$  on both benchmarks, demonstrating superior alignment between the prompt generator and segmenter. Notably, on the WheatIns dataset, which features dense occlusions, our method improves  $mAP$  by over 4.7% compared to the second best baseline (RS+Query). Such superiority mainly gains from our bi-level optimization strategy, which can prevent the alignment overfitting and improve the generalization. Beyond accuracy, Table 1 also highlights the parameter efficiency of our approach. While automated prompting methods like USIS and RSPrompter introduce auxiliary networks (up to 100M+ trainable parameters) or require fine-tuning the massive SAM backbone, BLO-Inst

Table 3. Comparison of BLO-Inst with baselines on biomedical benchmarks. Metrics reported are Mean AP ( $mAP$ ),  $AP_{50}$ , and  $AP_{75}$  (%). Best results are highlighted in **bold**.

Method	CellCountIns			RWCellIns		
	$mAP$	$AP_{50}$	$AP_{75}$	$mAP$	$AP_{50}$	$AP_{75}$
Mask R	42.0	74.9	41.6	63.2	90.5	76.7
SOLO	41.6	63.7	37.4	64.7	89.5	74.6
SAM+B	50.9	82.3	60.4	76.1	91.6	88.2
SAM+M	49.7	74.2	50.9	75.0	91.8	84.7
RS+Anchor	49.8	78.7	55.2	76.1	92.5	88.1
RS+Query	38.0	58.0	42.4	71.5	90.4	83.4
USIS	34.8	67.6	33.2	74.3	90.8	85.2
<b>BLO-Inst</b>	<b>55.1</b>	<b>83.7</b>	<b>62.5</b>	<b>78.5</b>	<b>94.6</b>	<b>89.8</b>

achieves state-of-the-art performance with only 38.66M trainable parameters. This is achieved by freezing the SAM backbone and only updating the lightweight LoRA layers and the YOLO detector. Consequently, our training cost (0.51 GPU hours) is significantly lower or comparable than other SAM-based fine-tuning approaches, validating that our bi-level strategy maintains a high computational efficiency while improving model’s performance.

**Multi-class General Object Benchmarks.** We next evaluate performance on multi-class segmentation tasks using TransIns (Cars vs. LaneLines) and CarPartsIns (Wheels vs. Windows vs. Body, etc.). Results are summarized in Table 2. BLO-Inst consistently outperforms baselines in these complex scenarios. On CarPartsIns, which requires fine-grained discrimination between geometrically distinct components, our method achieves an  $AP_{75}$  of 67.2%, significantly surpassing the best automated prompting baseline, RS+Query (64.7%). This indicates that our bi-level optimization effectively teaches the detector to generate class-discriminative prompts, bounding boxes, that not only localize the object but are tightly fitted to trigger the specific semantic mask within SAM’s decoder.

**Biomedical Benchmarks.** Finally, to assess domain generalization, we report results on the CellCountIns and RW-



Figure 3. Qualitative Results on Natural Scenes (PennFudanPed). Comparison of instance segmentation performance. Our method (far right) produces sharper masks and handles occlusions more effectively than baselines.

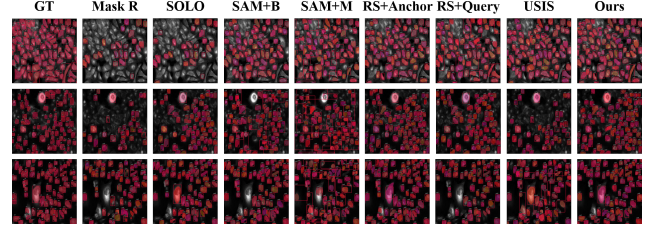


Figure 4. Qualitative Results on Biomedical Imagery (Cell-CountIns). In this challenging dense microscopy task, BLO-Inst successfully separates tightly packed and overlapping cells, whereas other baselines tend to merge adjacent instances.

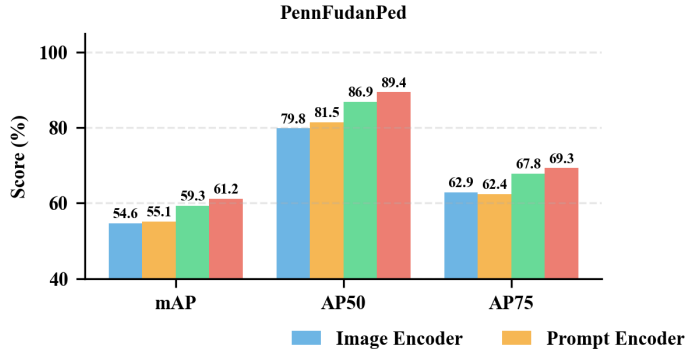
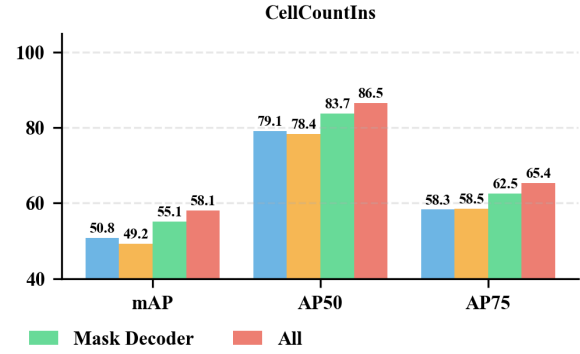


Figure 5. Effect of Trainable Components. Comparison of fine-tuning different modules of SAM on PennFudanPed and CellCountIns datasets. Updating the mask decoder yields the optimal balance between accuracy and parameter efficiency.

CellIns datasets in Table 3. Despite the significant domain gap between natural images and microscopy, BLO-Inst demonstrates robust adaptability. On the multi-class RW-CellIns dataset, our method achieves a remarkable 94.6%  $AP_{50}$  and 89.8%  $AP_{75}$ , outperforming the other automated prompting baselines (which may suffer alignment overfitting) and the specialist Mask R-CNN. This confirms that our method successfully bridges the domain gap, aligning the detector’s prompting strategy with the geometric properties of biomedical objects to achieve high-fidelity segmentation.

**Qualitative Analysis.** To visualize the effectiveness of BLO-Inst, we present qualitative comparisons against state-of-the-art baselines in Figure 3 and Figure 4. On the PennFudanPed dataset, traditional fully supervised methods like Mask R-CNN often struggle with precise boundary adherence, while recent automated prompting methods (e.g., USIS) occasionally exhibit prompt misalignment leading to fragmented masks. In contrast, BLO-Inst produces sharp, cohesive masks that accurately delineate instances even under occlusion. Furthermore, in the challenging high-density environment of CellCountIns, baseline prompt-learning approaches (e.g., RSPrompter) frequently suffer from “instance merging,” where adjacent cells are grouped into a single mask. Our method successfully separates these tightly packed instances with high fidelity, demonstrating that our bi-level alignment strategy effectively teaches the detector to generate discriminative prompts tailored to the specific segmentation properties of the SAM backbone. Additional qual-



itative results on traffic, agriculture, and industrial datasets are provided in the Appendix E.

#### 4.4. Ablation Studies

To validate the contributions of individual components and design choices in BLO-Inst, we conduct extensive ablation studies on the PennFudanPed and CellCountIns datasets. Unless otherwise stated, all ablations use the default settings: fine-tuning the mask decoder by LoRA, using first-order optimization, and a 1:1 data split ratio.

**Effectiveness of Trainable Components.** We first investigate which modules of the SAM should be optimized to adapt to downstream tasks. We compare four settings: updating the image encoder, prompt encoder, mask decoder, or all three components. As illustrated in Figure 5, fine-tuning the heavy image encoder yields suboptimal performance (e.g., 54.6% mAP on PennFudanPed) and incurs high training costs. This is attributed to the fact that the original image encoder, having been pre-trained on the massive SA-1B dataset, already possesses highly robust and generalizable feature extraction capabilities. Consequently, aggressively fine-tuning this backbone on small downstream datasets offers diminishing returns compared to the computational overhead. In contrast, updating the mask decoder alone significantly boosts performance to 59.3%, proving that adapting the segmentation head is crucial for aligning SAM with the prompt generator. While fine-tuning all components yields a marginal further gain (61.2%), it comes at a

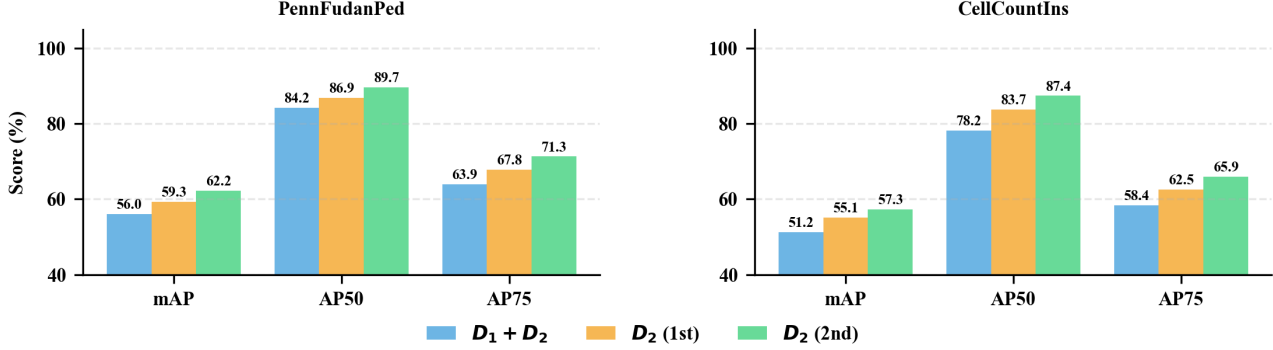


Figure 6. Optimization Strategy Analysis. Performance comparison between single-level training ( $D_1 + D_2$ ) and bi-level optimization. The proposed bi-level strategy significantly prevents overfitting compared to the baseline.

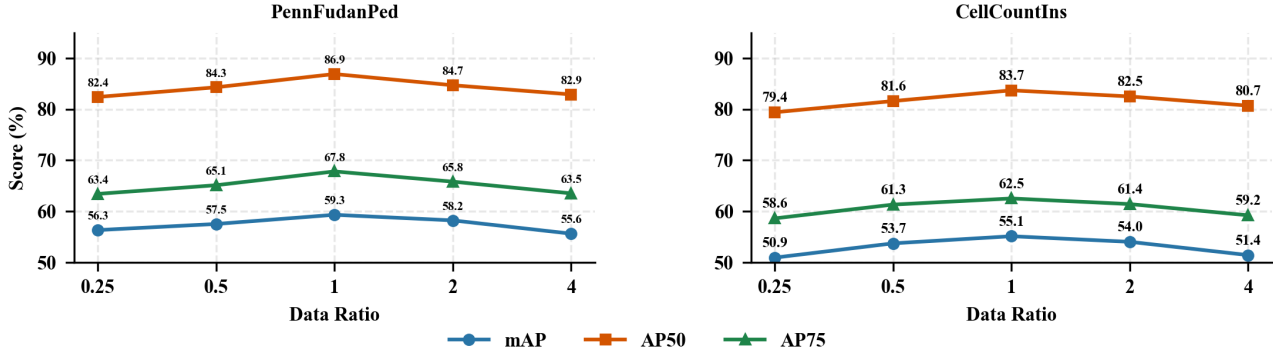


Figure 7. Sensitivity to Data Split Ratio. Mean AP performance across varying ratios ( $\gamma$ ) of subset ( $D_1$ ) to subset ( $D_2$ ). A balanced split ( $\gamma = 1$ ) proves most effective for convergence.

massive parameter cost. Thus, we select the mask decoder as the optimal trade-off between efficiency and accuracy.

**Impact of Optimization Strategy.** We analyze the effectiveness of our bi-level optimization strategy by comparing it against a standard single-level baseline (“ $D_1 + D_2$ ”), where the detector and segmenter are trained jointly on the union of datasets. We also compare first-order, “ $D_2$  (1st)”, with second-order, “ $D_2$  (2nd)”, bi-level optimization, as shown in Figure 6. The results demonstrate that the bi-level optimization ( $D_2$ ) strategies consistently outperform the single-level baseline (56.0% mAP) for both tasks. This confirms that splitting the data and using the segmenter’s validation loss to update the detector prevents overfitting and improves generalization. Although the second-order approximation achieves the highest performance (62.2% mAP) on pedestrian segmentation task, it requires significantly more computational resources. Therefore, we utilize the first-order optimization as our default setting to reduce training cost, while maintaining competitive accuracy.

**Sensitivity to Data Split Ratio.** Finally, we explore the impact of the data split ratio between the subset  $D_1$  (for  $\Theta$ ) and subset  $D_2$  (for  $\Phi$ ). We test ratios of  $\gamma = |D_1|/|D_2|$  ranging from 0.25 to 4. As shown in Figure 7, a balanced split ( $\gamma = 1$ ) yields the best performance (59.3% mAP on PennFudanPed). Skewing the data too heavily towards the

subset for segmenter updating (Ratio 4) starves the optimization process of detector, leading to poor prompt generation (dropping to 55.6%). Conversely, skewing towards the subset for detector updating (Ratio 0.25) prevents the segmenter from learning adequate domain adaptations. A balanced ratio provides sufficient data for both levels of the optimization to converge effectively.

## 5. Conclusion

In this paper, we presented BLO-Inst, a parameter-efficient instance segmentation framework that aligns the SAM with a pretrained detector through bi-level optimization. By formulating the prompt generator as a learnable “hyperparameter” optimized to maximize SAM’s validation performance, we establish a cooperative feedback loop that bridges the objective gap between geometric localization and segmentation map prediction. Extensive experiments across six diverse benchmarks, including challenging biomedical microscopy, demonstrate that BLO-Inst significantly outperforms both fully supervised specialist models and state-of-the-art automated prompting approaches. These findings validate bi-level optimization as a robust paradigm for adapting foundation models to complex downstream tasks, offering a promising direction for future research in automated prompt learning.

## Impact Statement

This paper presents a method for combining large-scale foundation models with smaller, task-specific models. By proposing a bi-level optimization strategy to effectively align these different architectures, our work enables the creation of highly accurate systems tailored for specific tasks without the need to retrain the entire large model. This approach promotes sustainable AI practices by reducing the energy consumption required for model adaptation. While our experiments highlight the potential for accelerating progress in specialized fields like biomedical microscopy, we acknowledge that advancements in high-performance segmentation could also be applied to surveillance technologies. We believe the primary impact of our work lies in enabling more efficient and targeted use of foundation models.

## References

atri. cell dataset. <https://universe.roboflow.com/atri-gly8b/cell-p3pcx>, nov 2023. URL <https://universe.roboflow.com/atri-gly8b/cell-p3pcx>. visited on 2026-01-02.

Benigmim, Y., Roy, S., Essid, S., Kalogeiton, V., and Lathuilière, S. Collaborating foundation models for domain generalized semantic segmentation. In *Proceedings of the IEEE/CVF Conference on Computer Vision and Pattern Recognition*, pp. 3108–3119, 2024.

Bottou, L. Large-scale machine learning with stochastic gradient descent. In *Proceedings of COMPSTAT'2010: 19th International Conference on Computational StatisticsParis France, August 22-27, 2010 Keynote, Invited and Contributed Papers*, pp. 177–186. Springer, 2010.

Chen, C., Zheng, S., Chen, X., Dong, E., Liu, X. S., Liu, H., and Dou, D. Generalized dataweighting via class-level gradient manipulation. *Advances in Neural Information Processing Systems*, 34:14097–14109, 2021.

Chen, K., Liu, C., Chen, H., Zhang, H., Li, W., Zou, Z., and Shi, Z. Rsprompter: Learning to prompt for remote sensing instance segmentation based on visual foundation model. *IEEE Transactions on Geoscience and Remote Sensing*, 62:1–17, 2024.

Cheng, B., Misra, I., Schwing, A. G., Kirillov, A., and Girdhar, R. Masked-attention mask transformer for universal image segmentation. In *Proceedings of the IEEE/CVF conference on computer vision and pattern recognition*, pp. 1290–1299, 2022.

Cheng, T., Song, L., Ge, Y., Liu, W., Wang, X., and Shan, Y. Yolo-world: Real-time open-vocabulary object detection. In *Proceedings of the IEEE/CVF conference on computer vision and pattern recognition*, pp. 16901–16911, 2024.

Choe, S. K., Neiswanger, W., Xie, P., and Xing, E. Betty: An automatic differentiation library for multilevel optimization. *arXiv preprint arXiv:2207.02849*, 2022.

Devlin, J., Chang, M.-W., Lee, K., and Toutanova, K. Bert: Pre-training of deep bidirectional transformers for language understanding. *arXiv preprint arXiv:1810.04805*, 2018.

Finn, C., Abbeel, P., and Levine, S. Model-agnostic meta-learning for fast adaptation of deep networks. In *Proceedings of the 34th International Conference on Machine Learning*, volume 70, pp. 1126–1135, 2017.

Gong, T., Chen, K., Wang, X., Chu, Q., Zhu, F., Lin, D., Yu, N., and Feng, H. Temporal roi align for video object recognition. In *Proceedings of the AAAI Conference on Artificial Intelligence*, volume 35, pp. 1442–1450, 2021.

Grazzi, R., Franceschi, L., Pontil, M., and Salzo, S. On the iteration complexity of hypergradient computation. In *International Conference on Machine Learning*, 2020.

He, K., Gkioxari, G., Dollár, P., and Girshick, R. Mask r-cnn. In *Proceedings of the IEEE international conference on computer vision*, pp. 2961–2969, 2017.

Hosseini, R., Zhang, L., Garg, B., and Xie, P. Fair and accurate decision making through group-aware learning. In *International Conference on Machine Learning*, pp. 13254–13269. PMLR, 2023.

Houlsby, N., Giurgiu, A., Jastrzebski, S., Morrone, B., De Laroussilhe, Q., Gesmundo, A., Attariyan, M., and Gelly, S. Parameter-efficient transfer learning for nlp. In *International conference on machine learning*, pp. 2790–2799. PMLR, 2019.

Hu, E. J., Shen, Y., Wallis, P., Allen-Zhu, Z., Li, Y., Wang, S., Wang, L., and Chen, W. Lora: Low-rank adaptation of large language models. *arXiv preprint arXiv:2106.09685*, 2021.

Jia, M., Tang, L., Chen, B.-C., Cardie, C., Belongie, S., Hariharan, B., and Lim, S.-N. Visual prompt tuning. In *European conference on computer vision*, pp. 709–727. Springer, 2022.

Kim, M. and Hospedales, T. A stochastic approach to bi-level optimization for hyperparameter optimization and meta learning. In *Proceedings of the AAAI Conference on Artificial Intelligence*, volume 39, pp. 17913–17920, 2025.

Kirillov, A., Mintun, E., Ravi, N., Mao, H., Rolland, C., Gustafson, L., Xiao, T., Whitehead, S., Berg, A. C., Lo, W.-Y., et al. Segment anything. In *Proceedings of the IEEE/CVF international conference on computer vision*, pp. 4015–4026, 2023.

learning, M. cell count dataset. <https://universe.roboflow.com/machine-learning-potko/cell-count-m2j3t>, mar 2024. URL <https://universe.roboflow.com/machine-learning-potko/cell-count-m2j3t>. visited on 2026-01-02.

Li, C., Sultan, R. I., Khanduri, P., Qiang, Y., Indrin, C., and Zhu, D. Autoprosam: Automated prompting sam for 3d multi-organ segmentation. In *2025 IEEE/CVF Winter Conference on Applications of Computer Vision (WACV)*, pp. 3570–3580. IEEE, 2025.

Lian, S., Zhang, Z., Li, H., Li, W., Yang, L. T., Kwong, S., and Cong, R. Diving into underwater: Segment anything model guided underwater salient instance segmentation and a large-scale dataset. In *International Conference on Machine Learning*, pp. 29545–29559. PMLR, 2024.

Liu, H., Simonyan, K., and Yang, Y. Darts: Differentiable architecture search. *arXiv preprint arXiv:1806.09055*, 2018a.

Liu, R., Gao, J., Zhang, J., Meng, D., and Lin, Z. Investigating bi-level optimization for learning and vision from a unified perspective: A survey and beyond. *IEEE Transactions on Pattern Analysis and Machine Intelligence*, 44(12):10045–10067, 2021.

Liu, R., Mu, P., Yuan, X., Zeng, S., and Zhang, J. A general descent aggregation framework for gradient-based bi-level optimization. *IEEE Transactions on Pattern Analysis and Machine Intelligence*, 45(1):38–57, 2022.

Liu, S., Qi, L., Qin, H., Shi, J., and Jia, J. Path aggregation network for instance segmentation. In *Proceedings of the IEEE conference on computer vision and pattern recognition*, pp. 8759–8768, 2018b.

Liu, S., Zeng, Z., Ren, T., Li, F., Zhang, H., Yang, J., Jiang, Q., Li, C., Yang, J., Su, H., et al. Grounding dino: Marrying dino with grounded pre-training for open-set object detection. In *European conference on computer vision*, pp. 38–55. Springer, 2024.

Pasupa, K., Kittiworapanya, P., Hongnern, N., and Woraratpanya, K. Evaluation of deep learning algorithms for semantic segmentation of car parts. *Complex & Intelligent Systems*, 8(5):3613–3625, 2022.

Radford, A., Narasimhan, K., Salimans, T., Sutskever, I., et al. Improving language understanding by generative pre-training. *OpenAI*, 2018.

Redmon, J., Divvala, S., Girshick, R., and Farhadi, A. You only look once: Unified, real-time object detection. In *Proceedings of the IEEE conference on computer vision and pattern recognition*, pp. 779–788, 2016.

Ren, S., He, K., Girshick, R., and Sun, J. Faster r-cnn: Towards real-time object detection with region proposal networks. *Advances in neural information processing systems*, 28, 2015.

SEG. Trans dataset. <https://universe.roboflow.com/seg-ohfrw/trans-y9kyy>, mar 2023. URL <https://universe.roboflow.com/seg-ohfrw/trans-y9kyy>. visited on 2026-01-02.

Shehadeh, A. test dataset. <https://universe.roboflow.com/albara-shehadeh-o8han/test-0aige>, mar 2024. URL <https://universe.roboflow.com/albara-shehadeh-o8han/test-0aige>. visited on 2026-01-02.

Vaswani, A., Shazeer, N., Parmar, N., Uszkoreit, J., Jones, L., Gomez, A. N., Kaiser, Ł., and Polosukhin, I. Attention is all you need. *Advances in neural information processing systems*, 30, 2017.

Wang, L., Shi, J., Song, G., and Shen, L.-f. Object detection combining recognition and segmentation. In *Asian conference on computer vision*, pp. 189–199. Springer, 2007.

Wang, X., Zhang, R., Shen, C., Kong, T., and Li, L. Solo: A simple framework for instance segmentation. *IEEE transactions on pattern analysis and machine intelligence*, 44(11):8587–8601, 2020.

Wang, X., Zhang, R., Kong, T., Li, L., and Shen, C. Solov2: Dynamic and fast instance segmentation. *Advances in Neural information processing systems*, 33:17721–17732, 2021.

Wu, J., Wang, Z., Hong, M., Ji, W., Fu, H., Xu, Y., Xu, M., and Jin, Y. Medical sam adapter: Adapting segment anything model for medical image segmentation. *Medical image analysis*, 102:103547, 2025.

Yang, Q., Peng, J., and Chen, D. A review of research on instance segmentation based on deep learning. In *International Conference on Computer Engineering and Networks*, pp. 43–53. Springer, 2023.

Yi, J., Wu, P., Jiang, M., Huang, Q., Hoeppner, D. J., and Metaxas, D. N. Attentive neural cell instance segmentation. *Medical image analysis*, 55:228–240, 2019.

Zhang, K. and Liu, D. Customized segment anything model for medical image segmentation. *arXiv preprint arXiv:2304.13785*, 2023.

Zhang, L., Liang, Y., Zhang, R., Javadi, A., and Xie, P. Blo-sam: bi-level optimization based finetuning of the

segment anything model for overfitting-preventing semantic segmentation. In *Proceedings of the 41st International Conference on Machine Learning*. JMLR.org, 2024.

Zhang, L., Garg, B., Sridhara, P., Hosseini, R., and Xie, P. Learning from mistakes: A multi-level optimization framework. *IEEE Transactions on Artificial Intelligence*, 2025.

Zhou, D., Fang, J., Song, X., Liu, L., Yin, J., Dai, Y., Li, H., and Yang, R. Joint 3d instance segmentation and object detection for autonomous driving. In *Proceedings of the IEEE/CVF Conference on Computer Vision and Pattern Recognition*, pp. 1839–1849, 2020.

Zhou, K., Yang, J., Loy, C. C., and Liu, Z. Learning to prompt for vision-language models. *International Journal of Computer Vision*, 130(9):2337–2348, 2022.

Zhou, M., He, C., Wang, R., and Chen, X. Ov3d-cg: Open-vocabulary 3d instance segmentation with contextual guidance. In *Proceedings of the IEEE/CVF International Conference on Computer Vision*, pp. 5305–5314, 2025.

## A. Objective Function

For both the lower-level and upper-level optimization steps, we utilize a unified multi-task objective function  $\mathcal{L}_{total}$ . This objective combines the detection losses required to maintain YOLO’s localization capabilities with the segmentation loss required for SAM’s mask generation. The total loss is defined as:

$$\mathcal{L}_{total} = \lambda_1 \mathcal{L}_{box} + \lambda_2 \mathcal{L}_{obj} + \lambda_3 \mathcal{L}_{cls} + \lambda_4 \mathcal{L}_{seg} \quad (5)$$

where  $\lambda$  terms are hyper-parameters governing the weight of each component. The individual loss components are calculated as follows:

- **Box Regression Loss ( $\mathcal{L}_{box}$ ):** We employ the Complete Intersection over Union (CIoU) loss to penalize bounding box errors. For a predicted box  $b_{pred}$  and target box  $b_{gt}$ :

$$\mathcal{L}_{box} = 1 - \text{CIoU}(b_{pred}, b_{gt}) \quad (6)$$

- **Objectness and Classification Loss ( $\mathcal{L}_{obj}$ ,  $\mathcal{L}_{cls}$ ):** We use Binary Cross-Entropy (BCE) with logits to supervise objectness and class probabilities. To address class imbalance, we adopt the Focal Loss formulation:

$$\mathcal{L}_{obj/cls} = -\alpha(1 - p_t)^\gamma \log(p_t) \quad (7)$$

where  $p_t$  is the predicted probability of the target class, and  $\alpha, \gamma$  are hyperparameters modulating the loss contribution of hard and easy examples.

- **Segmentation Loss ( $\mathcal{L}_{seg}$ ):** This is the critical link between the two models. We compute the pixel-wise Binary Cross-Entropy between the predicted mask  $M_{pred}$  and the ground truth mask  $M_{gt}$ . Crucially, to focus the loss on the relevant instance, we crop the loss calculation to the region defined by the bounding box  $\mathbf{b}$ :

$$\mathcal{L}_{seg} = \frac{1}{|\mathbf{b}|} \sum_{(i,j) \in \mathbf{b}} \text{BCE}(M_{pred}^{(i,j)}, M_{gt}^{(i,j)}) \quad (8)$$

The deployment of this unified multi-task objective confers a critical dual advantage. First, the inclusion of standard detection losses ( $\mathcal{L}_{box}$ ,  $\mathcal{L}_{obj}$ ,  $\mathcal{L}_{cls}$ ) acts as a geometric anchor, preventing the detector from degenerating. Without these constraints, the detector might learn to exploit the segmenter’s biases, generating trivial or physically implausible prompts (e.g., encompassing the entire image) solely to minimize segmentation error, thereby losing its ability to distinguish distinct instances. Second, the integration of the segmentation loss ( $\mathcal{L}_{seg}$ ) transforms the optimization landscape, forcing the detector to seek a solution that is segmentation-optimal for both tasks. Unlike standard multi-task learning, where losses are simply summed during a single training phase, our bi-level formulation ensures that the detection parameters are updated specifically to minimize the validation risk of the segmenter, effectively encoding downstream mask fidelity into the bounding box regression coordinates.

## B. Detailed Optimization Algorithm

In this section, we offer a detailed description of the optimization algorithm of BLO-Inst. We employ a gradient-based optimization algorithm to tackle the problem outlined in Eq. (4). Drawing inspiration from Liu et al. (2018a), we approximately update  $\Theta^*(\Phi)$  via one-step gradient descent in the lower-level optimization. Then we plug the approximate  $\Theta^*(\Phi)$  into the learning process of the detector in the upper level and update  $\Phi$  via one-step gradient descent. By using the one-step gradient descent updates for the bi-level optimization framework, we reduce the computational complexity. The detailed derivation of the update is as follows.

**Inner Loop Adaptation (Lower Level).** In the inner loop, we aim to estimate how the segmenter  $\Theta$  adapts to the prompts generated by the current detector  $\Phi^{(t)}$ . Instead of a full training cycle, we compute a surrogate parameter  $\Theta^{(t+1)}$  by performing a single gradient descent step on the support set  $D_1$ . Given the current state  $\Theta^{(t)}$  and learning rate  $\alpha$ , this virtual update is defined as:

$$\Theta^{(t+1)} = \Theta^{(t)} - \alpha \nabla_{\Theta} \mathcal{L}_{total}(\Theta^{(t)}, \Phi^{(t)}; D_1) \quad (9)$$

**Outer Loop Alignment (Upper Level).** In the outer loop, we optimize the detector  $\Phi$  by minimizing the validation loss on  $D_2$ , conditioned on the adapted segmenter  $\Theta^{(t+1)}$ . This formulation effectively forces the detector to anticipate the segmenter’s reaction to its prompts. The detector update, with learning rate  $\beta$ , is given by:

$$\Phi^{(t+1)} = \Phi^{(t)} - \beta \nabla_{\Phi} \mathcal{L}_{total}(\Theta^*(\Phi), \Phi^{(t)}; D_2) \quad (10)$$

To capture the dependency of the optimal segmenter  $\Theta^*$  on  $\Phi$ , we employ the unrolled differentiation method (Liu et al., 2018a). By substituting the one-step approximation from Eq. (9) into the upper-level objective, the gradient with respect to  $\Phi$  can be approximated as:

$$\nabla_{\Phi} \mathcal{L}_{total}(\Theta^*(\Phi), \Phi) \approx \nabla_{\Phi} \mathcal{L}_{total}(\Theta - \alpha \nabla_{\Theta} \mathcal{L}_{total}(\Theta, \Phi), \Phi) \quad (11)$$

Applying the chain rule to this unrolled objective reveals that the total gradient consists of a direct gradient term and an implicit Hessian-vector product term:

$$\nabla_{\Phi} \mathcal{L}_{total}(\Theta - \alpha \nabla_{\Theta} \mathcal{L}_{total}, \Phi) = \nabla_{\Phi} \mathcal{L}_{D_2}(\Theta^*, \Phi) - \alpha \nabla_{\Phi, \Theta}^2 \mathcal{L}_{D_1}(\Theta, \Phi) \cdot \nabla_{\Theta} \mathcal{L}_{D_2}(\Theta^*, \Phi) \quad (12)$$

where  $\mathcal{L}_{D_1}$  and  $\mathcal{L}_{D_2}$  denote the losses computed on the support and query sets, respectively.

**Hessian Approximation.** Computing the mixed second-derivative matrix  $\nabla_{\Phi, \Theta}^2$  directly is computationally expensive. To circumvent this, we approximate the Hessian-vector product in the second term of Eq. (12) using a finite difference method. This reduces the complexity to just two forward passes:

$$\nabla_{\Phi} \mathcal{L}_{D_2}(\Theta^*, \Phi) - \alpha \nabla_{\Phi, \Theta}^2 \mathcal{L}_{D_1}(\Theta, \Phi) \cdot \nabla_{\Theta} \mathcal{L}_{D_2}(\Theta^*, \Phi) \approx \frac{\nabla_{\Phi} \mathcal{L}_{D_1}(\Theta^+, \Phi) - \nabla_{\Phi} \mathcal{L}_{D_1}(\Theta^-, \Phi)}{2\epsilon} \quad (13)$$

Here,  $\Theta^{\pm} = \Theta \pm \epsilon \nabla_{\Theta^*} \mathcal{L}_{D_2}(\Theta^*, \Phi)$  represents the segmenter weights perturbed in the direction of the upper-level gradient, and  $\epsilon$  is a small scalar (e.g.,  $\epsilon = 0.01 / \|\nabla_{\Theta^*} \mathcal{L}_{D_2}(\Theta^*, \Phi)\|_2$ ).

**Optimization Order.** The parameter  $\alpha$  acts as a switch between first-order and second-order optimization. Setting  $\alpha = 0$  yields a first-order approximation (ignoring the Hessian term), which significantly reduces computational cost. For our primary experiments, we utilize this first-order optimization for efficiency and stability, but we provide an ablation analysis of the full second-order scheme in the experimental section.

## C. Datasets

To evaluate the effectiveness and generalization capability of BLO-Inst across diverse domains, we conduct comprehensive experiments on six datasets that vary significantly in object density, scale, and class complexity. These datasets are categorized into general object benchmarks and biomedical benchmarks, ensuring a robust assessment of the model’s adaptability. The statistics of the datasets are listed in Table 4.

Table 4. Number of data examples in different tasks

Dataset	PennFudanPed	TransIns	WheatIns	CarPartsIns	CellCountIns	RWCellIns
Train size	74	135	392	400	219	126
Test size	96	59	170	100	32	212

In the realm of general object segmentation, we utilize three distinct binary benchmarks. First, the PennFudanPed <sup>1</sup> dataset serves as a standard benchmark for pedestrian detection and segmentation. It represents a binary task (Pedestrian vs. Background) that rigorously tests the model’s ability to handle articulated deformations and frequent occlusions typical of urban environments. Second, we employ the TransIns <sup>2</sup> dataset, which focuses on vehicle detection within transportation surveillance contexts. This benchmark evaluates the model’s performance on rigid objects under varying lighting and traffic conditions. Third, we include the WheatIns <sup>3</sup> (global wheat detection) dataset, an agricultural benchmark characterized by

<sup>1</sup>[https://www.cis.upenn.edu/~jshi/ped\\_html/](https://www.cis.upenn.edu/~jshi/ped_html/)

<sup>2</sup><https://universe.roboflow.com/seg-ohfrw/trans-y9kyy/dataset/1>

<sup>3</sup><https://universe.roboflow.com/albara-shehadeh-o8han/test-oaige>

extremely high object density and severe overlaps. This dataset challenges the model to effectively distinguish crowded instances where standard detectors often fail due to aggressive suppression.

To assess fine-grained semantic capabilities, we utilize the CarPartsIns<sup>4</sup> dataset. Unlike the previous binary tasks, this is a multi-class benchmark requiring the segmentation of specific vehicle components such as wheels, lights, windows, and the car body. This task is particularly significant as it tests the model’s capacity for hierarchical semantic differentiation, requiring it to generate distinct prompts for sub-components that possess vastly different aspect ratios and geometric shapes within a single object category.

Finally, we evaluate domain generalization using two biomedical microscopy datasets. CellCountIns<sup>5</sup> is a binary benchmark designed for cell counting and segmentation. It features small, dense, and visually similar instances with low contrast against the background, highlighting the effectiveness of our bi-level fine-tuning in bridging the domain gap between natural scenes and microscopy. Complementing this is the RWCellIns<sup>6</sup> dataset, a multi-class biomedical benchmark that distinguishes between red and white blood cells. This task introduces the challenge of biological class distinction, testing whether the detector can learn to generate class-discriminative prompts to separate biological structures that share similar circular geometries but differ in texture and size.

## D. Additional Ablation Study

**End-to-End vs. Separate Training.** We validate the necessity of our unified training pipeline in Figure 8. In the “Separate” setting, we first train the YOLO detector to convergence and then freeze it to train the SAM segmenter. In the “End-to-End” setting, both are updated simultaneously by the bi-level optimization framework. The results reveal that end-to-end training yields significant improvements (+6.2% mAP on PennFudanPed). In the separate approach, the detector learns to optimize bounding boxes solely, which does not necessarily correlate with the optimal prompts for SAM. Our end-to-end approach allows the detector to learn how to prompt SAM specifically to maximize mask quality, creating a synergistic feedback loop.

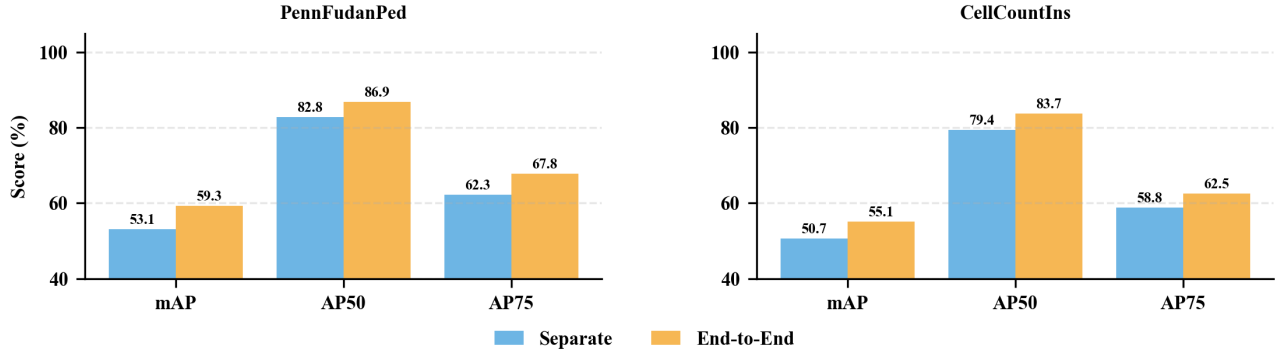


Figure 8. End-to-End vs. Separate Training. Jointly optimizing the detector and segmenter via the bi-level feedback loop (End-to-End) consistently outperforms the sequential (Separate) training pipeline.

## E. Additional Qualitative Results

To further demonstrate the versatility of BLO-Inst, as shown in Figure 9, Figure 10, Figure 12, and Figure 11, we provide qualitative comparisons on four additional benchmarks covering traffic scenes, agriculture, and industrial inspection.

<sup>4</sup><https://universe.roboflow.com/kmitl-yjl9y/car-parts-segmentation>

<sup>5</sup><https://universe.roboflow.com/machine-learning-potko/cell-count-m2j3t/dataset/3>

<sup>6</sup><https://universe.roboflow.com/atri-gly8b/cell-p3pcx>



Figure 9. Traffic Scenes (TransIns). Segmentation of vehicles in complex lighting conditions.

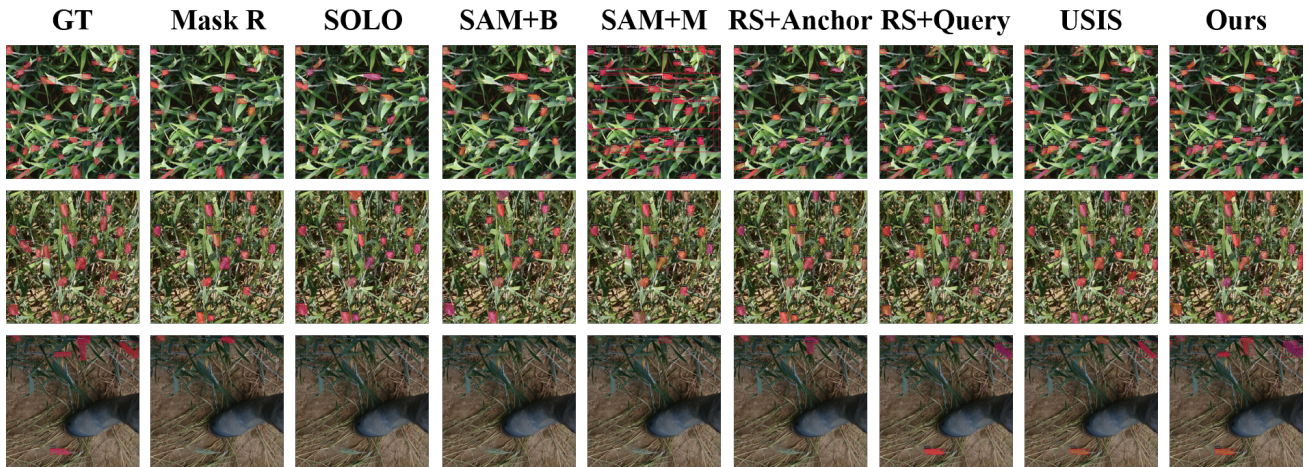


Figure 10. Agriculture (Wheat). Dense instance segmentation of wheat heads in field imagery.



Figure 11. Industrial Inspection (CarParts). Fine-grained segmentation of vehicle components.

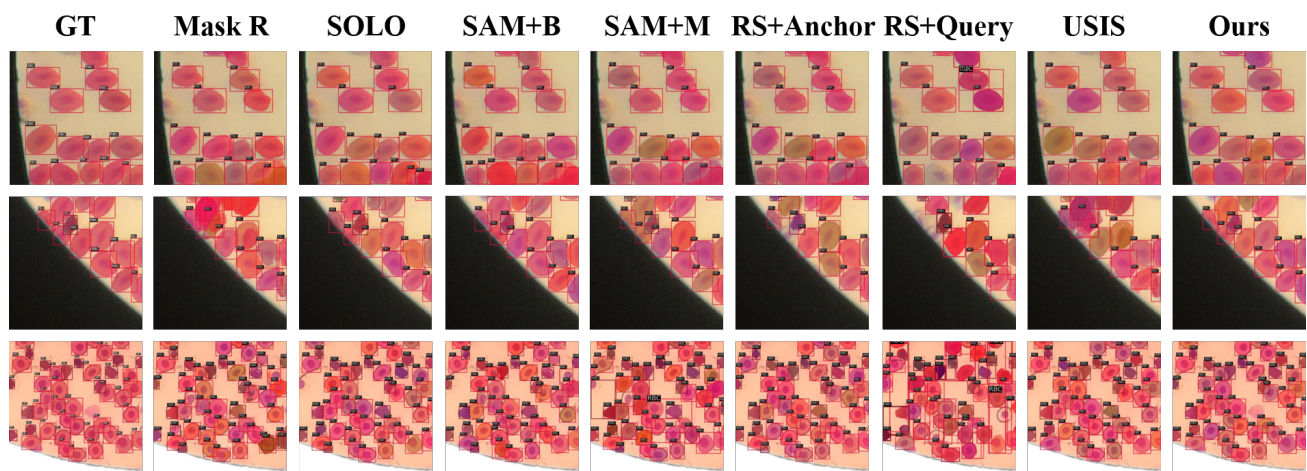


Figure 12. Medical Hematology (RW-Cell). Segmentation of red and white blood cells.